PAPER

Check for updates

Construction of glutathione-responsive paclitaxel prodrug nanoparticles for image-guided targeted delivery and breast cancer therapy†

Weiwei Ma, [ID] * Qiufeng Zhao, Shilong Zhu, Xinyue Wang, Chuangchuang Zhang, Daming Ma, Na Li* and Yanyan Yin*

Paclitaxel (PTX) remains an essential drug in the treatment of breast cancer. To improve metabolic stability and real-time monitoring of drug location, we develop a visualized nano-prodrug. Novel hyaluronic acid (HA)-coated glutathione (GSH)-sensitive chitosan (CS)-based nano-prodrug (HA/TPE-CS-SS-PTX NPs) with aggregation-induced emission effects (AIE) were accomplished. The prodrug NPs (drug loading 29.32%, particle size 105 nm, regular sphericity) exhibit excellent fluorescence stability. The prodrug NPs could target tumor cells with high expression of CD44 and decompose in the presence of high concentrations of glutathione. *In vitro* evaluations revealed that the prodrug NPs have significant cytotoxicity on 4T1 cells, and due to their excellent AIE characteristics, their position in cells can be tracked. Moreover, the prodrug NPs also shown superior anti-tumor effects *in vivo* experimental. Overall, the HA/TPE-CS-SS-PTX NPs we constructed have excellent bio-imaging capabilities and can be served as a potential nanomedicine for PTX delivery against breast cancer.

1. Introduction

Paclitaxel (PTX) is a broad-spectrum and highly effective anti-cancer drug[1,2] that stabilizes microtubules during cell division, inhibits microtubule depolymerization, and leads to tumor cell apoptosis.[3,4] As a broad-spectrum anti-cancer drug, paclitaxel has therapeutic effects on ovarian cancer, lung cancer, breast cancer, colon cancer, lymphoma, melanoma, and other tumors.[5] However, due to poor water solubility, low bioavailability, allergic reactions, and significant side effects caused by injection assisted solvents, the clinical application of paclitaxel still faces many problems.[6,7] In the past few decades, nano-medicine has become a valid cancer treatment strategy to overcome these issues.[8,9]

Recent research on drug delivery system (nano-DDS) emphasizes versatility, which enables targeted delivery and triggered release of drugs within targeted cells, as well as real-time monitoring of drug positioning.[10,11] Most nano-DDS are designed to encapsulate chemotherapeutic drugs or fluorescent dye into carrier for treatment and visualization. However, non-covalent encapsulation has been criticized for its poor stability, low drug delivery efficiency, and premature leakage of drug or fluorescent dye in the systemic circulation.[12,13] Consequently, these issues urge us to develop a particular visualized prodrug to improve metabolic stability and real-time monitoring of drug location.

Polysaccharide based nano prodrugs have attracted wide-spread attention due to their clear component, accurate structure, stable drug loading capacity, and efficient anti-tumor activity.[14,15] Chitosan (CS) is a natural non-toxic polymer material with good biodegradability and biocompatibility, which has been widely used in the delivery of anti-tumor drugs for cancer diagnosis and therapy.[16,17] In addition, CS has a large number of amino groups ($-NH_2$) and hydroxyl groups ($-OH$), which are excellent modification sites for functionalization.[18] If hydrophobic anticancer drugs are directly coupled to hydrophilic polymer chains through covalent bonds, it can greatly prevent premature drug release. However, cationic nanoparticles formed based on chitosan not only lack tumor targeting effects, but also susceptible to serum protein-mediated aggregation and elimination.[19] Hyaluronic acid has natural electronegativity and can be used to encapsulate cationic-based nanoparticles. Meanwhile, hyaluronic acid has been used in drug delivery systems due to its low immunogenicity, high biocompatibility and targeting of tumor-specific expression receptors (cluster determinant 44, CD44).[20] Therefore, HA functionalized drug delivery systems can actively target cancer cells.[21,22]

Traditional fluorescent dyes are greatly limited in biological imaging because of the aggregation induced quenching effect (ACQ).[23] Fortunately, the appearance of aggregation induced emission (AIE) dyes, which have the opposite effect to aggregation induced quenching, provides a possibility to overcome this defect.[24] Tang *et al.* reported the aggregation-induced emission
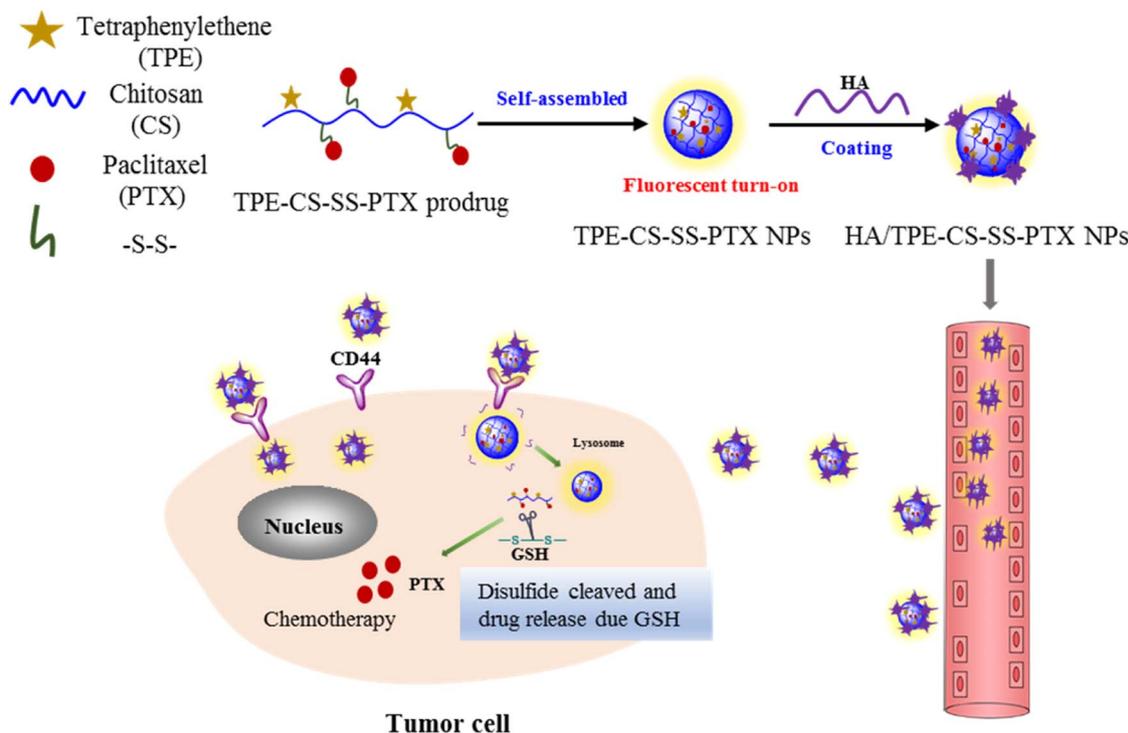
Fig. 1 Schematic representation the intravenous delivery of HA-decorated nano-prodrug (HA/TPE-CS-SS-PTX NPs) and their GSH-triggered drug release in cancer cells.

effect in 2001,[25] tetraphenylethene (TPE) is a typical group with aggregation-induced emission effect, which has attracted great attention recently.[26,27] In recent years, fluorescent nanoparticles based on AIE active chromophores have turn into a new generation of biological imaging nanoparticles.[28] It will be very interesting to develop fluorescent nano-prodrug composed of luminophor with AIE characteristics as alternative fluorescent materials for cell imaging and drug delivery monitoring.

In this work, we developed a simple and efficient nano-prodrug. The HA-coated redox sensitive visualized nano-prodrug HA/TPE-CS-SS-PTX were exploited in order to highly efficient treatment of cancer and real-time monitoring of drug localization. We choose chitosan as the skeleton to develop a visualized GSH-activated prodrug of PTX. PTX was grafted onto the chitosan skeleton *via* –S–S– bond (Fig. 1), which is stable under normal physiologic conditions but decomposes at high intracellular glutathione (GSH) concentrations. At the same time, TPE is also attached to chitosan by covalent bonds. The AIE-based prodrug self-assembles to form nanoparticles, which were then coated with hyaluronic acid. The HA/TPE-CS-SS-PTX NPs are expected to possess an outstanding AIE feature, selectively gather in the tumor site, effectively internalized into tumor cells through CD44-mediated endocytosis and complete glutathione triggering PTX release in the cytoplasm. Herein, the preparation, synthesis and characterization of HA/TPE-CS-SS-PTX NPs were studied. In addition, a detailed evaluation was conducted on the AIE active cell imaging, cell uptake, and *in vitro* and *in vivo* anti-tumor efficacy of HA/TPE-CS-SS-PTX NPs.

2. Materials and methods
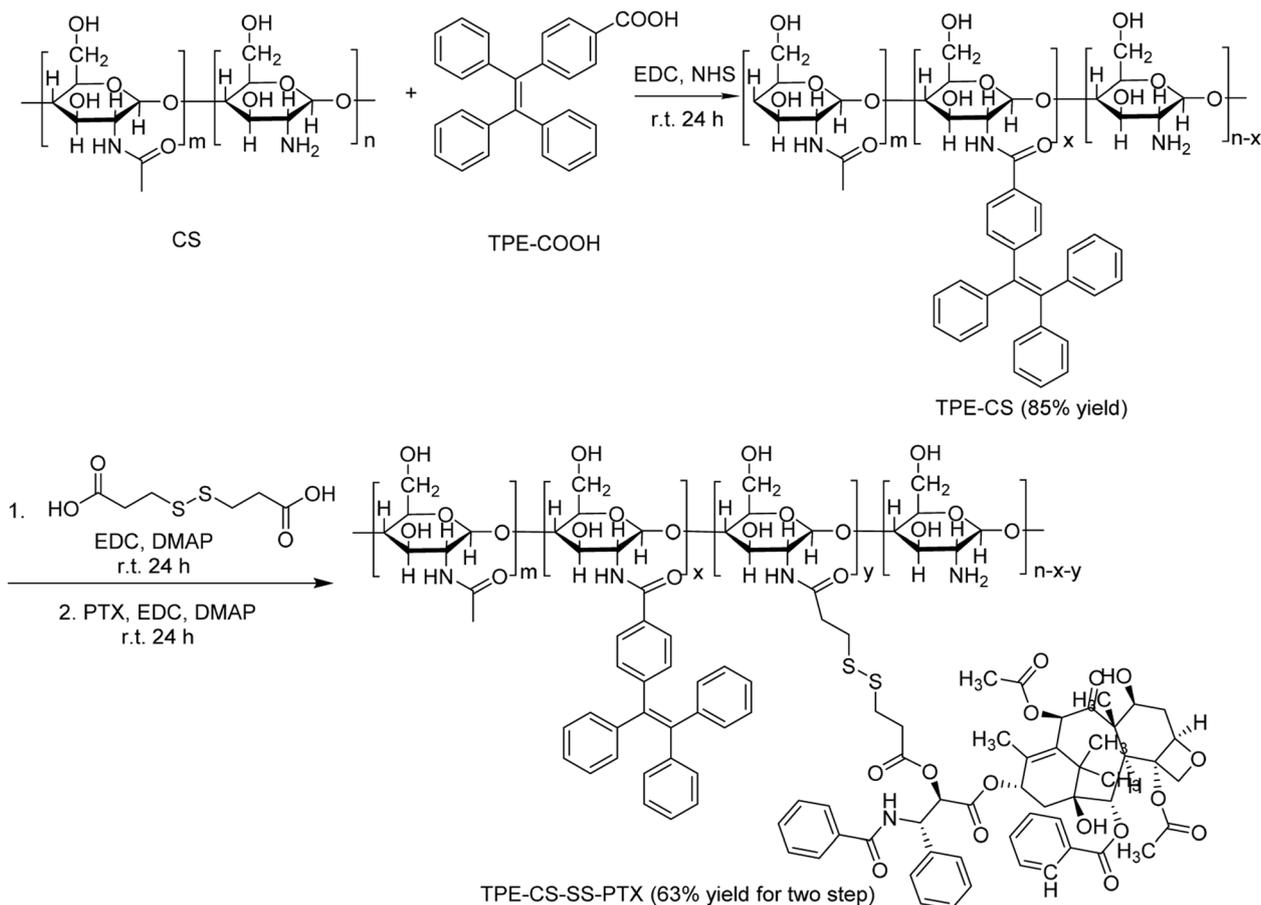
2.1. Materials

Chitosan (CS, 30 kDa, 95% deacetylated), 1-ethyl-3-(3-(dimethylamino) propyl) carbodiimide hydrochloric acid salt (EDC·HCl), N-hydroxysuccinimide (NHS), 3,3′-dithiodipropionic acid (DPA), and 4-dimethylaminopyridine (DMAP) were purchased from Aladdin Reagent Co. Ltd. Sodium HA (molecular weights 10 kDa) was purchased from Freda Biochem Co. Ltd. Paclitaxel (PTX, purity of 99.9%) was purchased from Adamas Co. Ltd. TPE-COOH was purchased from Alfa Chemical Co. Ltd.

The mouse breast cancer 4T1 cells were kindly provided by the Department of Pharmacology, Xinxiang Medical University. The Cells were cultured at 37 °C and 5% CO_2 in high-glucose DMEM containing 10% fetal bovine serum (FBS), 1% penicillin, and 1% streptomycin. Specific pathogen-free Kunming mice (weighing 18–22 g, 5–6 weeks old) were supplied by Laboratory Animal Center of Xinxiang Medical University.

2.2. Synthesis of TPE-CS-SS-PTX

The synthesis of conjugates is shown in Scheme 1. First, TPE were introduced onto CS *via* the amidation reaction between TPE-COOH and CS. Precisely, TPE-COOH (10 mg) in dry formamide (10 mL) was added EDC (15 mg) and NHS (10 mg) at room temperature, then the reaction mixture was stirred 3 h under inert atmosphere. Subsequently, the CS (100 mg) in N,N-Dimethylformamide (DMF, 5 mL) solution was added slowly to the TPE-COOH containing mixture and stirring for another 24 h at room temperature. After the completion of the reaction, the

Scheme 1 Synthetic route of TPE-CS-SS-PTX prodrug.

mixture was purified by dialysis (MW, 10 KD) against distilled water for 2 days and freeze-dried to give TPE-CS.

Second, 3,3′-dithiodipropionic acid (DPA, 21 mg), 1-ethyl-3-(3-(dimethylamino) propyl) carbodiimide hydrochloric acid salt (EDC, 10 mg), 4-dimethylaminopyridine (DMAP, 12 mg) dissolved in an appropriate amount of anhydrous DMF, the mixture was stirred under nitrogen protection for 3 h. After addition of TPE-CS (100 mg) in formamide (5 mL), the reaction mixture was continuously stirred for 24 h at room temperature. The residue was purified by dialysis (MW, 10 KD) against water for 2 days and freeze-dried. Following, the lyophilized product, EDC (10 mg), DMAP (12 mg) dissolved in an appropriate amount of anhydrous DMF, the mixture was stirred under nitrogen protection for 3 h. Then the solution of PTX (100 mg) in anhydrous DMF (2 mL) was added slowly to the mixture. The reaction mixture was continuously stirred at room temperature for 24 hours. After the completion of the reaction, the mixture was purified by dialysis (MW, 10 KD) against distilled water for 2 days and freeze-dried to give TPE-CS-SS-PTX.

The chemical structure and functional groups of TPE-CS-PTX were confirmed through FT-IR and ^{1}H NMR. ^{1}H NMR spectra were recorded on Bruker Avance/400 (^{1}H: 400 MHz at 25 °C) and TMS as internal standard. For FT-IR spectra, the samples were mixed with KBr and pressed. IR spectra was recorded from 500 to 4000 cm^{-1} at room temperature. The

molecular weight of TPE-CS-SS-PTX were calculated using the Gel Permeation Chromatography (GPC) method with Waters GPC 1515 (Waters, America) (column: Waters Styragel HT4). The mobile phase consisted of water and acetic acid (95 : 5 by volume). The flow rate was 0.7 mL min^{-1}.

2.3. Fabrication of HA/TPE-CS-SS-PTX nanoparticles

The nanoparticles were prepared by a probe-type ultrasonic method. The TPE-CS-SS-PTX was placed in a beaker (100 mg mL^{-1}, PBS), stirred at room temperature for 0.5 hours, and then ultrasonicated in an ice bath at 100 W with a probe ultrasound for 0.5 hours. Then pass 0.45 μM filter membrane filtration removes large aggregates to obtain a uniform precursor nanoparticle dispersion. The suspension was freeze-dried to obtain the solid powder of TPE-CS-SS-PTX nanoparticles.

HA is coated outside the TPE-CS-SS-PTX nanoparticles through electrostatic interactions. To put it simply, the TPE-CS-SS-PTX nanoparticles is slowly added to the HA solution (1 mg mL^{-1}) and vigorously stirred at different weight ratios. The mixture was then maintained for 30 minutes at 37 °C.

2.4. Research on AIE features

The AIE characteristic of HA/TPE-CS-SS-PTX NPs in a series of different contents was studied. With an excitation wavelength of

321 nm, the fluorescence emission spectra were collected within the range of 220–600 nm. In order to visually observe the behavior of AIE, the sample was photographed under the ultraviolet light of 365 nm. In addition, irradiate (365 nm) the sample (0.1 mg mL^{-1}) continuously for 30 minutes, measure the fluorescence intensity change, and examine the photostability of HA/TPE-CS-SS-PTX NPs.

2.5. Description of HA/TPE-CS-SS-PTX NPs

The particle size, polymer dispersion index (PDI), and zeta potential of HA/TPE-CS-SS-PTX prodrug nanoparticles were measured by a Nano-ZS90 Malvern Mastersizer (Malvern Instruments Ltd, Malvern, UK). The morphology of prodrug NPs was observed by transmission electron microscopy (TEM) (JEOL, Japan). The drug load (DL) is determined by HPLC (Waters 2796, USA) (column: Waters Symmetry C$_{18}$). The mobile phase consisted of acetonitrile and water (1.8 : 1.2 by volume). The concentration of PTX was measured at a wavelength of 230 nm with a flow rate of 1.0 mL min^{-1}.

$$DL(\%) = \frac{\text{Weight of PTX in NPs}}{\text{Weight of PTX loaded NPs}} \times 100\%$$

2.6. Stability and hemolysis test

To investigate the storage stability, the solution of HA/TPE-CS-SS-PTX NPs (1 mg mL^{-1} in PBS) was stored studied at 4 °C and 37 °C. At the appropriate times (0, 2, 4, 6, 8, 10, 24 and 48 h), the size distribution and PDI of HA/TPE-CS-SS-PTX NPs were monitored by DLS at 25 °C.

The hemolysis test is a method for evaluating biocompatibility of the HA/TPE-CS-SS-PTX NPs on red blood cells. Appropriate amount of blood was centrifuged at 2000 rpm for 5 min to separate the erythrocytes from plasma. The supernatant was taken out and the precipitated erythrocyte pellet was washed with PBS (pH 7.4) three times. In the following step, the erythrocyte pellet was re-suspended in PBS in 1 : 10 ratio (erythrocytes: PBS, w/v). 0.5 mL of diluted erythrocyte pellet suspension was added to each tube. The erythrocyte suspension dissolved in water and PBS represented 100% and 0% hemolysis, respectively. HA/TPE-CS-SS-PTX NPs with different concentrations were added to the test tubes at the final concentration: 100, 200, 300, 400, and 500 μg mL^{-1}. After 4 hours of culture at 37 °C, the samples were centrifuged to remove the unlysed erythrocytes.

Take out the supernatant of all samples and the optical density (OD) of released hemoglobin were measured at $\lambda = 540$ nm with ELISA-reader. The percent hemolysis was determined by the following equation:

$$\text{Hemolysis (\%)} = (OD_{sample} - OD_0)/(OD_{100} - OD_0)$$

where OD_{sample} is the supernatant absorbance of the sample, OD_0, and OD_{100} are the supernatant absorbance of a solution of 0% and 100% hemolysis, respectively.

2.7. *In vitro* PTX release behavior of nano-prodrug

2 mL of HA/TPE-CS-SS-PTX (1 mg mL^{-1}) prodrug NPs was added to a dialysis bag, and then dipped into 50 mL of a pH 7.4 PBS releasing medium with 0 or 10 mM GSH. The dialysis samples were incubated in a constant temperature shaker at 37 °C and 200 rpm for 24 h. 2 mL volume of solution was taken out at the given interval, and 2 mL of fresh medium was replenished. The concentration of PTX released into medium was measured by HPLC.

2.8. Cellular uptake test

The uptake of prodrug NPs into 4T1 cells was detected using confocal laser scanning microscopy (CLSM) and flow cytometry. For CLSM analysis, 4T1 cells (5×10^4 cells per mL) were inoculated in a glass plate and incubated for 24 hours. Then, the cells were placed in a fresh medium containing HA/TPE-CS-SS-PTX nanoparticles (100 μg mL^{-1}) and incubated for 1, 2, or 4 hours. Then the cells were washed three times with cold PBS. Next, used Hoechst 33 342 (10 μg mL^{-1}) stained the nucleus for 10 min. The sample was observed under CLSM. In flow cytometry analysis, the above cell groups were washed three times with cold PBS, then suspended in PBS. Flow cytometry was used to detect the fluorescence intensity of TPE in cell samples.

2.9. Cytotoxicity assay

The cytotoxicity of CS, TPE-CS, TPE-CS-SS-PTX and HA/TPE-CS-SS-PTX NPs to 4T1 cells were determined by MTT methods. 4T1 cells were seeded in 96-well plates with a density of 8000 cells per well. All the cells were added 100 μL DMEM culture medium and incubated at 37 °C in 5% CO$_2$ atmosphere for 24 h to induce cells adherence. Then removing the culture medium, different concentrations of CS, TPE-CS, TPE-CS-SS-PTX and HA/TPE-CS-SS-PTX NPs solutions in culture medium were prepared and added during cell inoculation, and the cells were incubated at 37 °C in 5% CO$_2$ atmosphere for another 24 hours.

Following, the culture media were removed, and 100 μL fresh DMEM media (containing 20 μL MTT, 5 mg mL^{-1}) was added into every well. After incubation at 37 °C for additional 4 h, the MTT solution was removed, and 100 μL of DMSO was added to dissolve formazan crystals. After the formazan was fully dissolved, the optical density of was measured at a wavelength of 490 nm. 4T1 cells cultured with culture media were chosen as controls, their viabilities were considered as 100%. And the relative cell viability (%) was indicated as a percentage relative to the untreated control cells.

2.10. *In vivo* antitumor activity

The animal procedures were performed in accordance with the Guidelines for Care and Use of Laboratory Animals of Xinxiang Medical University (Henan, China), and the experiments were approved by the Animal Ethics Committee of Xinxiang Medical University. To evaluate the antitumor efficacy of HA/TPE-CS-SS-PTX NPs, tumor model was established by subcutaneous injection of 1×10^6 4T1 cells into the right flank of Kunming mice. When the tumor volume reached approximately 50 mm^3,

the mice were randomly divided into five groups (6 mice per group) and intravenously injected with saline, TPE-CS (1 mg kg^{-1}), TPE-CS-SS-PTX (10 mg kg^{-1} PTX), HA/TPE-CS-SS-PTX NPs (10 mg kg^{-1} PTX) and PTX (10 mg kg^{-1}), all samples were dissolved in PBS. The tumor volume (length × width^2/2) and body weight were monitored every two days.

After 21 days treatment, the mice were sacrificed, the tumors and major organs including heart, kidney, liver, lung, spleen were collected. Calculated the tumor weight inhibition rate (IR) using the following equation:

$$IR = (W_{control} - W_{test})/W_{control,}$$

where $W_{control}$ and W_{test} represented the average tumor weight of the saline group and the treated groups, respectively. In addition, the tumor was subjected to H&E staining test for histological evaluation.

3.   Results and discussion

3.1.   Synthesis of TPE-CS-SS-PTX

The GSH-sensitive CS-based visualized amphiphilic prodrug was synthesized as following procedures (Scheme 1). First, the carboxyl group of TPE-COOH and the amino group on chitosan are linked together through amidation reaction to synthesize TPE-CS in 85% yield. Then DPA with disulfide bond was used as the GSH-sensitive linkage to conjugate TPE-CS to hydrophobic PTX through the formation of amide bonds and ester bonds in 63% yield.

3.2.   Characterization of TPE-CS-SS-PTX

^{1}H NMR analysis demonstrated the fabrication of TPE-CS-SS-PTX. As shown in Fig. 2A, in the spectrum of TPE-CS, the specific signal at 1.97 ppm was owed the methyl of acetyl groups

of *N*-acetyl glucosamine. The signal observed at 1.30 ppm was assigned to hydroxymethyl groups, and the signal 3.3 ppm was ascribed to the protons of the backbone of CS.[29] The typical signals of TPE were observed at 7.0–7.8 ppm, which confirmed the introduction of TPE (Fig. S1†). Compared with TPE-CS, several new signals appeared in the spectrum of TPE-CS-SS-PTX. The resonance peaks at 7.30–8.14 ppm were corresponding to the aromatic proton in PTX. The new signal at 2.5 ppm attributed to the methylene (–CH$_2$–) of 3,3′-dithiodipropionic acid (Fig. S2†). These results demonstrated PTX was successfully coupled with TPE-CS to form visualized prodrug TPE-CS-SS-PTX.

Moreover, FTIR analysis further confirmed the formation of TPE-CS-SS-PTX. As shown in Fig. 2B, in the spectrum of TPE-CS, the associated changes in the amide band (from 1643 cm^{-1} to 1615 cm^{-1}) were due to a newly formed amide bond between the carboxyl group of TPE-COOH and the amine group of CS, indicating the formation of TPE-CS. In the spectrum of TPE-CS-SS-PTX, the typical absorption bands of PTX (C=O ester, C=O amide at 1734 cm^{-1}, 1646 cm^{-1}) were indicated the successful fabrication of TPE-CS-SS-PTX.

To estimate the molecular weight distribution of TPE-CS-SS-PTX, its weight-average molecular weight (M_w) and number-average molecular weight (M_n) were measured by GPC, the results were shown in Table S1.† The weight-average molecular weight (M_w) of CS (M_w = 30.12 kDa, PDI = 1.10) by GPC was lower than that of TPE-CS-SS-PTX (M_w = 44.85 kDa, PDI = 1.46). The increased molecular weight signified the successful fabrication of TPE-CS-SS-PTX.

3.3.   Characterization of HA/TPE-CS-SS-PTX NPs

The obtained prodrugs were subsequently self-assembled through probe ultrasonic. The hydrodynamic diameter of the TPE-CS-SS-PTX NPs was determined as 90.44 ± 0.821 nm (PDI =
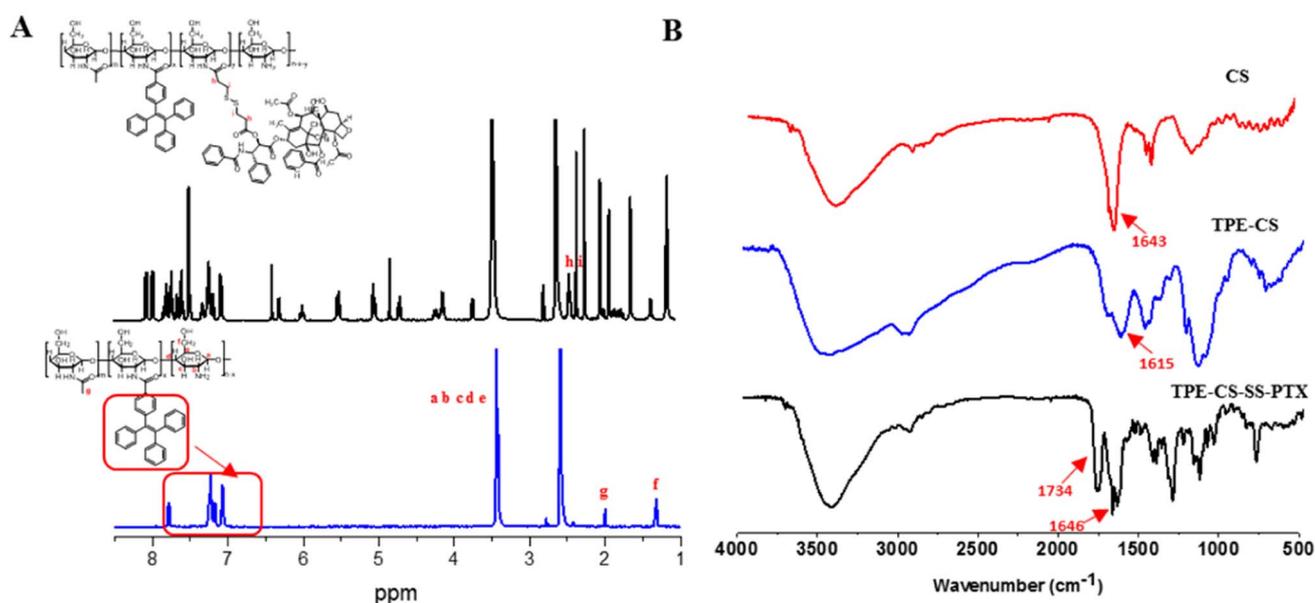

Fig. 2 ^{1}H NMR (A) and FT-IR (B) spectra of TPS–CS and TPE–CS–SS–PTX.

0.124) and the zeta potential was + 31.8 ± 2.35 mV. Then the HA/CS-TPE-SS-PTX nanoparticle was prepared through electrostatic attraction. When the mass ratio of HA and TPE-CS-SS-PTX NPs was fixed as 1/3, the particle size of HA/TPE-CS-SS-PTX nanoparticles was 105.3 ± 1.569 nm (PDI = 0.238), the zeta potential was + 27.8 ± 2.16 mV (Fig. 3A). The changes in particle size and potential also demonstrated the successful decoration of

hyaluronic acid on the TPE-CS-SS-PTX NPs. It is well known that particles about 100 nm in diameter can accumulate at the tumor tissue through enhanced permeability and retention effects.[30] In addition, due to the repulsive force between charges, the high zeta potential could potentially increase stability of the NPs. From HPLC analysis, the drug loading of the HA/TPE-CS-SS-PTX NPs were calculated as 29.32%.
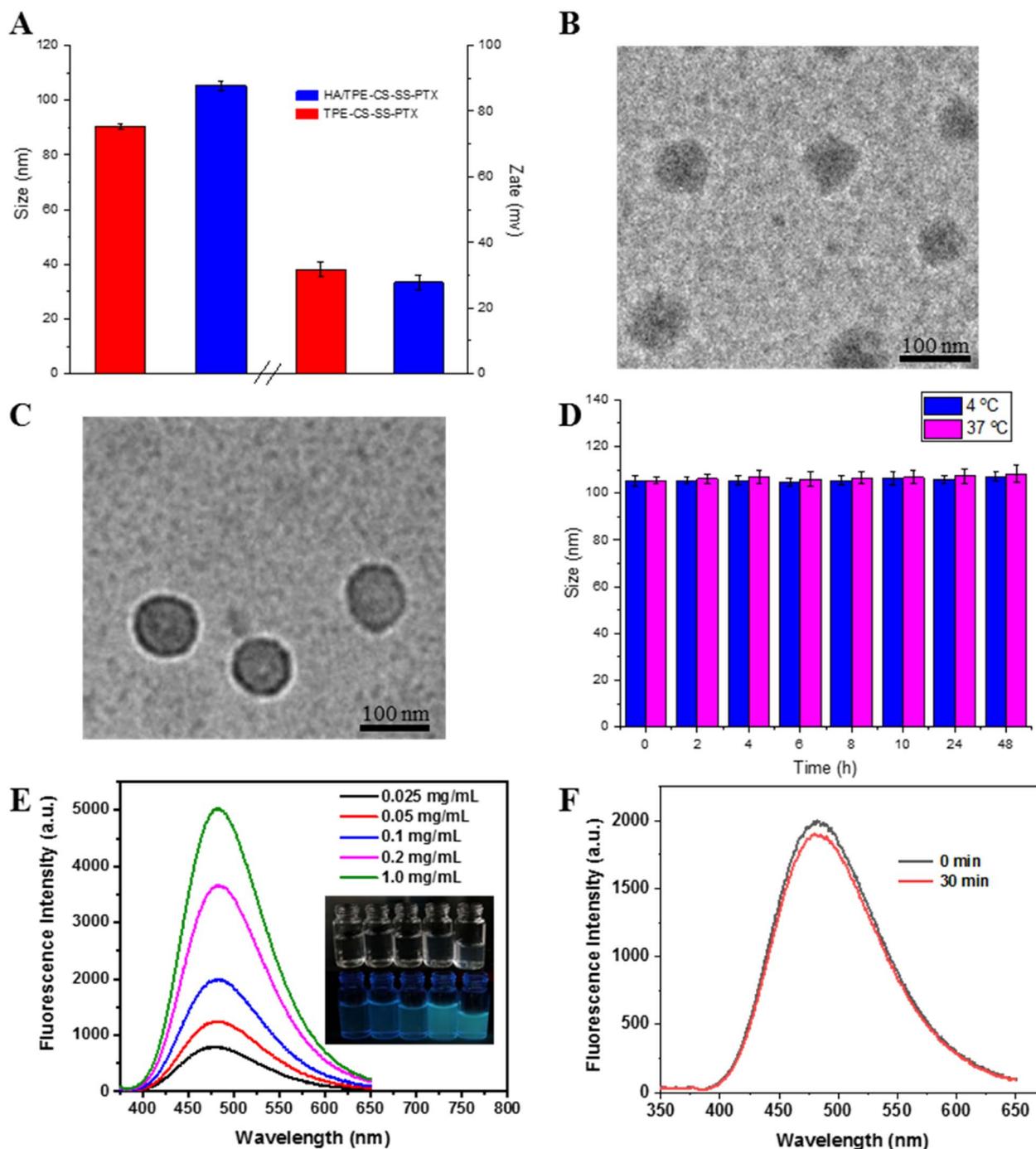

Fig. 3 Particle size distribution and zeta potential of HA/TPE-CS-SS-PTX NPs and TPE-CS-SS-PTX NPs (A). TEM images of TPE-CS-SS-PTX NPs (B). TEM images of HA/TPE-CS-SS-PTX NPs (C). Stability of HA/TPE-CS-SS-PTX NPs suspension for 0, 2, 4, 6, 8, 10, 24 and 48 h at 4 and 37 °C (D). Fluorescence emission spectra of HA/TPE-CS-SS-PTX NPs (Ex = 321 nm). Photostability of the HA/TPE-CS-SS-PTX NPs under UV light exposure at 365 nm (E). Fluorescence stability of HA/TPE-CS-SS-PTX NPs (0.1 mg mL^{-1}) for irradiated by UV at 365 nm for 30 minutes (F).

The TEM image shows spherical morphology of the core/shell and uniform size distribution ($\sim$90 nm) of TPE-CS-SS-PTX NPs (Fig. 3B) and HA/TPE-CS-SS-PTX NPs (Fig. 3C). The particle size measured by TEM is smaller than that measured by DLS, which is due to the collapse of micelles during TEM sampling and drying.

3.4. Stability of prodrug NPs

The instability of nanomedicine delivery systems hinders their usefulness in clinical applications.[31] To obtain the storage stability of HA/TPE-CS-SS-PTX NPs, their size distribution was monitored over time after incubation at 4 °C and 37 °C. As shown in Fig. 3D the NPs were stored at 4 °C for 48 h did not significant changes in their size. Similar phenomenon was observed when HA/TPE-CS-SS-PTX were stored at 37 °C. These results indicated that the HA/TPE-CS-SS-PTX NPs had excellent stability at 4 and 37 °C.

3.5. Optical spectra

TPE-CS-SS-PTX solid powder appears white under normal indoor lighting and emits strong blue-green fluorescence under UV irradiation (Fig. S3†). Following the fluorescence properties of HA/TPE-CS-SS-PTX NPs were studied qualitatively. As shown in Fig. 3E, the fluorescence intensity (emission at about 475 nm) increases with the concentration of HA/TPE-CS-SS-PTX NPs aqueous solution, which is consistent with the image taken with a handheld UV lamp under a 365 nm UV lamp (Fig. 3E). The results indicate that the HA/TPE-CS-SS-PTX NPs exhibits AIE characteristics, and the intramolecular rotation of the TPE portion is blocked, resulting in enhanced emission.[32]

In order to further evaluate the fluorescence stability of the nanoparticles, the nanoparticles (0.1 mg mL^{-1}) were continuously irradiated by UV at 365 nm for 30 minutes, the results were shown in the Fig. 3F. After UV irradiation, it is clear that only a negligible change in fluorescence intensity was observed, indicating that the HA/TPE-CS-SS-PTX NPs exhibit excellently stable fluorescence properties. This characteristic makes HA/TPE-CS-SS-PTX NPs a promising candidate for biological imaging and can be used for biomedical applications.

3.6. Hemolysis evaluation

To evaluate the safety of the prodrug NPs, a hemolysis analysis was performed. As shown in Fig. 4A, after 4 h of incubation, although hemolysis levels increase in a dose-dependent manner, the maximum value of prodrug NPs was still less than 5%, (only 3.95 ± 0.05% at 500 μg mL^{-1}), which was acceptable for intravenous administration.[33] These results indicate that the prodrug NPs have good blood compatibility and potential for its use in cell imaging and cancer treatment.

3.7. *In vitro* drug release of prodrug NPs

In vitro release of PTX from HA/TPE-CS-SS-PTX NPs was investigated under simulated redox environments of cancer cells. The PTX content was measured by HPLC. High expression of GSH in tumor cells has been reported to accelerate drug release.[34] In the presence or absence of 10 mM GSH, the drug release behavior of prodrug NPs was studied by dialysis. The result is shown in Fig. 4B, GSH increased the release rate of PTX, and the drug release rate was about 80.35% within 24 h, while the release rate of PTX without GSH was only 17.55%. GSH can break disulfide bonds in prodrug, thus promoting drug release. The results showed that the drug release of prodrug NPs was inhibited in the normal physiological environment, but accelerated in the reducing micro-environment intracellular. Therefore, the redox sensitive prodrug NPs with disulfide bonds can decrease drug leakage in low-reducing environments (blood circulation), while triggering drug release in high-reducing environments can increase target drug concentration.

3.8. Cytotoxicity and apoptosis assay

In order to preliminarily evaluate the anti-tumor activity of HA/TPE-CS-SS-PTX NPs, it's *in vitro* cytotoxicity to 4T1 cells was measured using MTT assay. TPE-CS and CS also performed cytotoxicity tests to evaluate the biocompatibility of the system. As shown in Fig. 4C, the TPE-CS did not exhibit any cytotoxicity, and the cell viability was greater than 90%, proving that TPE-CS have good biocompatibility. However, HA/TPE-CS-SS-PTX prodrug NPs can effectively inhibit the proliferation of 4T1 cells, with the increase of drug concentration, cell viability decreased significantly in the investigated range (Fig. 4D). In addition, the cytotoxicity of TPE-CS-SS-PTX NPs were slightly stronger than that of paclitaxel. This can be explained by the passive diffusion of paclitaxel into cells. On the contrary, due to the coated of HA, more HA/TPE-CS-SS-PTX NPs can be internalized into 4T1 cells through receptor mediated endocytosis, therefore exhibiting higher cytotoxicity. All the results indicate that HA/TPE-CS-SS-PTX NPs has greater potential in safe and effective drug delivery. Due to its good biocompatibility, AIE characteristics, and ability to inhibit tumor cells, HA/TPE-CS-SS-PTX NPs will be very suitable for bioimaging and cancer treatment.

3.9. Cellular uptake

To investigate whether AIE prodrug NPs exhibit self-tracking during drug administration, we conducted CLSM observations and further evaluated the cellular uptake behavior of HA/TPE-CS-SS-PTX NPs on 4T1 cells. Hoechst (blue) was employed to visualize the cell nucleus. As shown in Fig. 5A, 4T1 cells showed clear red fluorescence after incubation with HA/TPE-CS-SS-PTX NPs, which may be due to the excellent AIE properties of the prodrug NPs. The results show that the prodrug NPs has good biological imaging performance. In addition, the fluorescence intensity was enhanced as the culture time increased from 1 to 4 h, indicating the prodrug NPs were efficiently internalized into the breast cancer cells and the uptake process of the cells was carried out in a time-dependent manner. Quantitative evaluation of TPE fluorescence intensity through flow cytometry also validated the delivery of his prodrug NPs. Consistent with CLSM results, the fluorescence intensity of 4T1 cells treated with HA/TPE-CS-SS-PTX NPs increased over time (Fig. 5B). Based on the above results, it can be reasonably inferred that
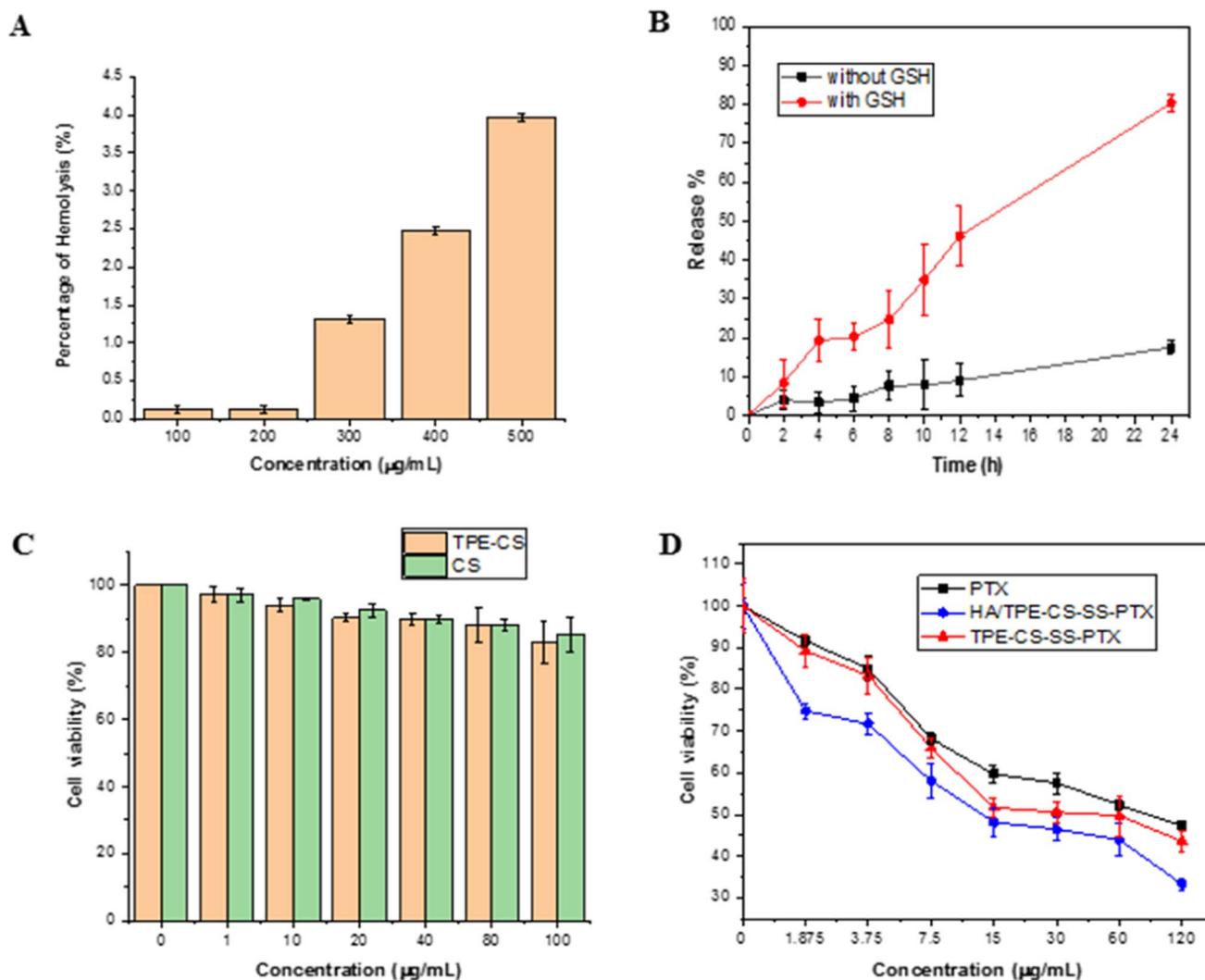
Fig. 4 Hemolysis rate of HA/TPE-CS-SS-PTX NPs at different concertation (A). *In vitro* release behavior of PTX from HA/TPE-CS-SS-PTX NPs with or without GSH (B). Cell viability of CS, TPE-CS (C) and PTX, TPE-CS-SS-PTX, HA/TPE-CS-SS-PTX NPs (D) toward the 4T1 cells by MTT assay. Triplicate experiments were performed each time.

HA/TPE-CS-SS-PTX NPs are promising for targeted drug delivery and bioimaging.

3.10. *In vivo* antitumor efficacy study

By conducting tumor growth inhibition studies on 4T1 tumor bearing mice, the anti-tumor activity of HA/TPE-CS-SS-PTX NPs were further evaluated. As shown in Fig. 6A, tumor growth was rapid in the PBS and TPE-CS group, while PTX, TPE-CS-SS-PTX and HA/TPE-CS-SS-PTX NPs showed considerable tumor suppression effect. However, HA/TPE-CS-SS-PTX NPs led to even smaller tumor sizes than those in the paclitaxel and TPE-CS-SS-PTX group.

After 21 days of treatment, the relative tumor size of the HA/TPE-CS-SS-PTX NPs group was 0.61 while the paclitaxel group was 2.05. The design of HA/TPE-CS-SS-PTX NPs is an important reason for the good anti-tumor effect of prodrug. Specifically, HA/TPE-CS-SS-PTX NPs can accumulate in tumors through EPR effects due to their nano-size of approximately 100 nm. Hyaluronic acid encapsulation can promote the entry of nanoparticles into tumor cells through receptor-mediated endocytosis. At the same time, the positive charge can bind the particles to the tumor surface (which is negatively charged) through electrostatic interactions. In tumor tissue, high concentrations of GSH trigger disulfide bond breaking in nanoparticles, which promotes drug release.[35] In conclusion, HA/TPE-CS-SS-PTX NPs showed excellent anti-tumor effects. In addition, as shown in Fig. 6B, similar to the PBS group, mice treated with HA/TPE-CS-SS-PTX NPs did not lose weight, indicating high biocompatibility of the prodrug nanoparticles, proving the prodrug NPs caused no harm to the mice and implied that prodrug NPs is a very promising tumor-targeting drug for cancer chemotherapy. The histological examination of the tumors was evaluated after 21 days of treatment. As shown in Fig. 6C, H&E staining of tumor tissues showed that
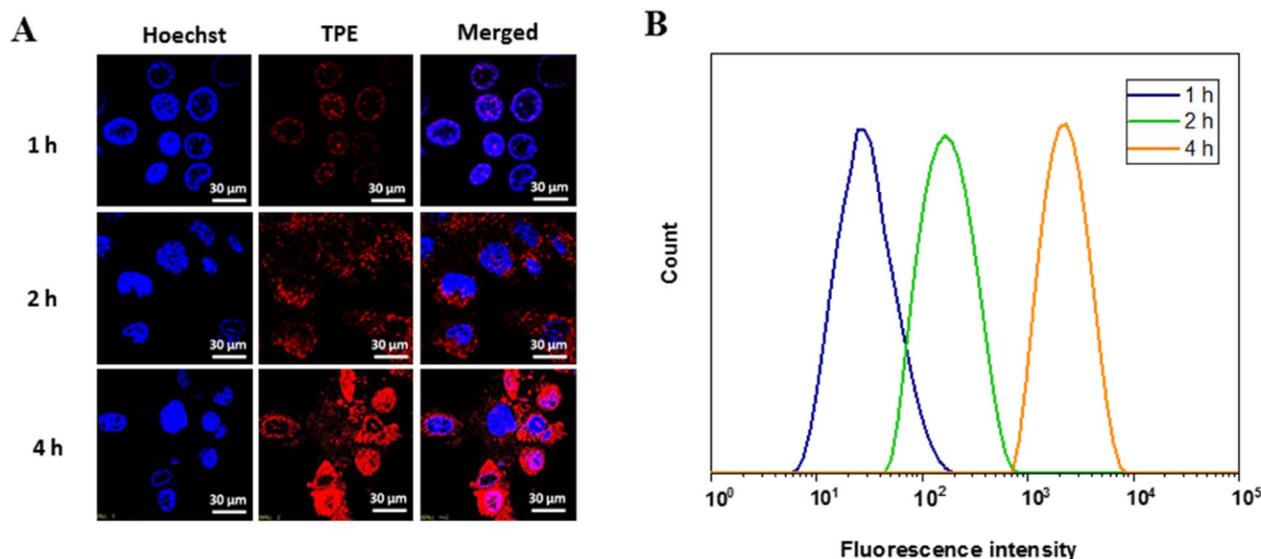
Fig. 5 CLSM images of 4T1 cells after incubation with HA/TPE-CS-SS-PTX for 1 h, 2 h, 4 h (A). Flow cytometric profiles of intracellular uptake of HA/TPE-CS-SS-PTX in 4T1 cells after 1 h, 2 h, 4 h (B).
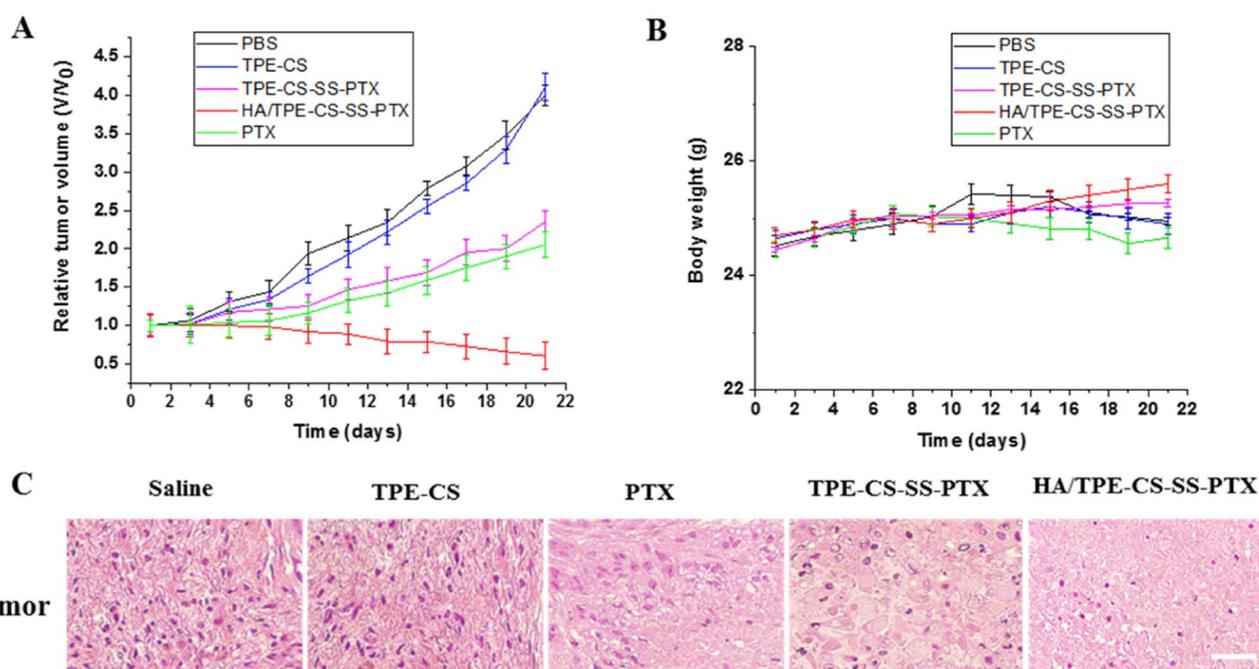

Fig. 6 Tumor volume changes of tumor-burdened mice (A). Body weight changes of tumor-burdened mice (B). H&E staining images of tumor from different groups after different treatments (C). The scale bars are 50 μm.

increased apoptosis of tumor cells was observed in the HA/TPE-CS-SS-PTX NPs group compared with other groups, further indicating the superior antitumor therapeutic efficacy of HA/TPE-CS-SS-PTX NPs.

4. Conclusion

In this study, we synthesized a novel visualized prodrug nanoparticle (HA/TPE-CS-SS-PTX NPs) with positive tumor targeting and GSH reaction properties. The prodrug NPs exhibited appropriate drug loading (29.32%), acceptable particle size (105 nm), regular sphericity, and excellent fluorescence stability. As expected, the prodrug NPs have good AIE characteristics, the fluorescence intensity gradually increased with the increase of concentration. *In vitro* drug release studies showed that GSH triggered the release pattern of the prodrug NPs (~80% within 24 h). *In vitro* and *in vivo* experiments proved the strongest antitumor efficacy of HA/TPE-CS-SS-PTX NPs compared with

PTX control. In a word, the conjugate prodrug NPs with aggregation-induced emission will be a potential candidate for biological imaging and cancer therapy.

Author contributions

WW Ma: conceptualization, methodology, visualization, projectadministration, funding acquisition, writing-review & editing; QF Zhao, SL Zhu, XY Wang, CC Zhang, DM Ma: methodology, validation, formal analysis, investigation, visualization, writing revision; N Li: funding acquisition, writing revision, experimental planning, material preparation; YY Yan: conceptualization, methodology, funding acquisition, writing-original draft.

Conflicts of interest

There is no conflict of interest.

Acknowledgements

References

1 Z. Zhang, L. Mei and S. S. Feng, Paclitaxel drug delivery systems, *Expert Opin. Drug Delivery*, 2013, **10**(3), 325–340, DOI: 10.1517/17425247.2013.752354.

2 M. Zhou, L. Wen, C. Wang, Q. Lei, Y. Li and X. Yi, Recent Advances in Stimuli-Sensitive Amphiphilic Polymer-Paclitaxel Prodrugs, *Front Bioeng. Biotechnol.*, 2022, **10**, 875034, DOI: 10.3389/fbioe.2022.875034.

3 B. M. Haynes, K. Cunningham and M. P. V. Shekhar, RAD6 inhibition enhances paclitaxel sensitivity of triple negative breast cancer cells by aggravating mitotic spindle damage, *BMC Cancer*, 2022, **22**(1), 1073, DOI: 10.1186/s12885-022-10119-z.

4 S. Tanaka, H. Miyazaki, A. Shiozaki, D. Ichikawa, E. Otsuji and Y. Marunaka, Cytosolic Cl- Affects the Anticancer Activity of Paclitaxel in the Gastric Cancer Cell Line, *MKN28 Cell. Cell Physiol. Biochem.*, 2017, **42**(1), 68–80, DOI: 10.1159/000477116.

5 C. Nehate, S. Jain, A. Saneja, *et al.*, Paclitaxel formulations: challenges and novel delivery options, *Curr. Drug Delivery*, 2014, **11**(6), 666–686, DOI: 10.2174/1567201811666140609154949.

6 Z. Xu, S. Zhu, M. Wang, Y. Li, P. Shi and X. Huang, Delivery of paclitaxel using PEGylated graphene oxide as a nanocarrier, *ACS Appl. Mater. Interfaces*, 2015, **7**(2), 1355–1363, DOI: 10.1021/am507798d.

7 F. Luo, Z. Fan, W. Yin, *et al.*, pH-responsive stearic acid-O-carboxymethyl chitosan assemblies as carriers delivering

small molecular drug for chemotherapy, *Mater. Sci. Eng., C*, 2019, **105**, 110107, DOI: 10.1016/j.msec.2019.110107.

8 S. Fu, G. Li, W. Zang, X. Zhou, K. Shi and Y. Zhai, Pure drug nano-assemblies: A facile carrier-free nanoplatform for efficient cancer therapy, *Acta Pharm. Sin. B*, 2022, **12**(1), 92–106, DOI: 10.1016/j.apsb.2021.08.012.

9 M. A. Barkat, S. Beg, F. H. Pottoo and F. J. Ahmad, Nanopaclitaxel therapy: an evidence based review on the battle for next-generation formulation challenges, *Nanomedicine*, 2019, **14**(10), 1323–1341, DOI: 10.2217/nnm-2018-0313.

10 F. Qiu, D. Wang, Q. Zhu, *et al.*, Real-time monitoring of anticancer drug release with highly fluorescent star-conjugated copolymer as a drug carrier, *Biomacromolecules*, 2014, **15**(4), 1355–1364, DOI: 10.1021/bm401891c.

11 L. Chen, B. Chen, X. Liu, *et al.*, Real-time monitoring of a controlled drug delivery system in vivo: construction of a near infrared fluorescence monomer conjugated with pH-responsive polymeric micelles, *J. Mater. Chem. B*, 2016, **4**(19), 3377–3386, DOI: 10.1039/c6tb00315j.

12 C. Chen, J. L. Zhou, X. Han, F. Song, X. L. Wang and Y. Z. Wang, A prodrug strategy based on chitosan for efficient intracellular anticancer drug delivery, *Nanotechnology*, 2014, **25**(25), 255101, DOI: 10.1088/0957-4484/25/25/255101.

13 M. I. Priester and T. L. M. Ten Hagen, Image-guided drug delivery in nanosystem-based cancer therapies, *Adv. Drug Delivery Rev.*, 2023, **192**, 114621, DOI: 10.1016/j.addr.202.

14 C. Zhang, Y. Song, G. Yan and J. Ma, Fluorinated carboxymethyl chitosan-based nano-prodrugs for precisely synergistic chemotherapy, *Int. J. Biol. Macromol.*, 2023, **227**, 252–261, DOI: 10.1016/j.ijbiomac.2022.12.157.

15 D. Li, T. Su, L. Ma, *et al.*, Dual-acidity-labile polysaccharide-di-drugs conjugate for targeted cancer chemotherapy, *Eur. J. Med. Chem.*, 2020, **199**, 112367, DOI: 10.1016/j.ejmech.2020.112367.

16 S. M. Matalqah, K. Aiedeh, N. M. Mhaidat, K. H. Alzoubi, Y. Bustanji and I. Hamad, Chitosan Nanoparticles as a Novel Drug Delivery System: A Review Article, *Curr. Drug Targets*, 2020, **21**(15), 1613–1624, DOI: 10.2174/1389450121666200711172536.

17 F. D. Moghaddam, E. N. Zare, M. Hassanpour, *et al.*, Chitosan-based nanosystems for cancer diagnosis and therapy: Stimuli-responsive, immune response, and clinical studies, *Carbohydr. Polym.*, 2024, **330**, 121839, DOI: 10.1016/j.carbpol.2024.121839.

18 V. Mikušová and P. Mikuš, Advances in Chitosan-Based Nanoparticles for Drug Delivery, *Int. J. Mol. Sci.*, 2021, **22**(17), 9652, DOI: 10.3390/ijms22179652.

19 M. Li, Y. Zhao, J. Sun, *et al.*, pH/reduction dual-responsive hyaluronic acid-podophyllotoxin prodrug micelles for tumor targeted delivery, *Carbohydr. Polym.*, 2022, **288**, 119402, DOI: 10.1016/j.carbpol.2022.119402.

20 F. Carton, Y. Chevalier, L. Nicoletti, *et al.*, Rationally designed hyaluronic acid-based nano-complexes for pentamidine delivery, *Int. J. Pharm.*, 2019, **568**, 118526, DOI: 10.1016/j.ijpharm.2019.118526.

21 J. Li, M. Huo, J. Wang, *et al.*, Redox-sensitive micelles self-assembled from amphiphilic hyaluronic acid-deoxycholic acid conjugates for targeted intracellular delivery of paclitaxel, *Biomaterials*, 2012, **33**(7), 2310–2320, DOI: **10.1016/j.biomaterials.2011.11.022**.

22 Y. Zhong, J. Zhang, R. Cheng, *et al.*, Reversibly crosslinked hyaluronic acid nanoparticles for active targeting and intelligent delivery of doxorubicin to drug resistant CD44+ human breast tumor xenografts, *J. Controlled Release*, 2015, **205**, 144–154, DOI: **10.1016/j.jconrel.2015.01.012**.

23 H. Shi, N. Liang, J. Liu, *et al.*, AIE-active polymeric micelles based on modified chitosan for bioimaging-guided targeted delivery and controlled release of paclitaxel, *Carbohydr. Polym.*, 2021, **269**, 118327, DOI: **10.1016/j.carbpol.2021.118327**.

24 Z. Wang, S. Chen, J. W. Lam, *et al.*, Long-term fluorescent cellular tracing by the aggregates of AIE bioconjugates, *J. Am. Chem. Soc.*, 2013, **135**(22), 8238–8245, DOI: **10.1021/ja312581r**.

25 J. Luo, Z. Xie, J. W. Lam, B. Z. Tang, *et al.*, Aggregation-induced emission of 1-methyl-1,2,3,4,5-pentaphenylsilole, *Chem. Commun.*, 2001, **18**, 1740–1741, DOI: **10.1039/b105159h**.

26 W. Z. Yuan, P. Lu, S. Chen, *et al.*, Changing the behavior of chromophores from aggregation-caused quenching to aggregation-induced emission: development of highly efficient light emitters in the solid state, *Adv. Mater.*, 2010, **22**(19), 2159–2163, DOI: **10.1002/adma.200904056**.

27 F. Qiao, J. Ke, Y. Liu, *et al.*, Cationic quaternized chitosan bioconjugates with aggregation-induced emission features for cell imaging, *Carbohydr. Polym.*, 2020, **230**, 115614, DOI: **10.1016/j.carbpol.2019.115614**.

28 L. Liang, T. Peng, X. Y. Geng, *et al.*, Aggregation-induced emission photosensitizer microneedles for enhanced melanoma photodynamic therapy, *Biomater. Sci.*, 2024, **12**(5), 1263–1273, DOI: **10.1039/d3bm01819a**.

29 Y. Han, N. Liang, P. Yan, Y. Kawashima, F. Cui and S. Sun, A Chitosan-Based Micellar System as Nanocarrier For the Delivery of Paclitaxel, *Polymers*, 2020, **12**(2), 380, DOI: **10.3390/polym12020380**.

30 K. Maruyama, Intracellular targeting delivery of liposomal drugs to solid tumors based on EPR effects, *Adv. Drug Delivery Rev.*, 2011, **63**(3), 161–169, DOI: **10.1016/j.addr.2010.09.003**.

31 B. Sun, C. Luo, H. Yu, X. Zhang, Q. Chen, W. Yang, M. Wang, Q. Kan, H. Zhang, Y. Wang, Z. He and J. Sun, Disulfide Bond-Driven Oxidation- and Reduction-Responsive Prodrug Nanoassemblies for Cancer Therapy, *Nano Lett.*, 2018, **18**, 3643–3650.

32 D. D. La, S. V. Bhosale, L. A. Jones and S. V. Bhosale, Tetraphenylethylene-Based AIE-Active Probes for Sensing Applications, *ACS Appl. Mater. Interfaces*, 2018, **10**(15), 12189–12216, DOI: **10.1021/acsami.7b12320**.

33 L. Mazzarino, G. Loch-Neckel, L. Dos Santos Bubniak, *et al.*, Nanoparticles Made From Xyloglucan-Block-Polycaprolactone Copolymers: Safety Assessment for Drug Delivery, *Toxicol. Sci.*, 2015, **147**(1), 104–115, DOI: **10.1093/toxsci/kfv114**.

34 B. Niu, K. Liao, Y. Zhou, *et al.*, Application of glutathione depletion in cancer therapy: Enhanced ROS-based therapy, ferroptosis, and chemotherapy, *Biomaterials*, 2021, **277**, 121110, DOI: **10.1016/j.biomaterials.2021.121110**.

35 X. Zhao, H. Guo, H. Bera, *et al.*, Engineering Transferrin-Decorated Pullulan-Based Prodrug Nanoparticles for Redox Responsive Paclitaxel Delivery to Metastatic Lung Cancer Cells, *ACS Appl. Mater. Interfaces*, 2023, **15**(3), 4441–4457, DOI: **10.1021/acsami.2c18422**.